

A Hybrid CMOS Photonic RF Channelizer: System Design and Analysis

Aly Moussa, *Student Member, IEEE*, and Vishal Saxena, *Senior Member, IEEE*

Abstract—Wireless perception requires processing of broadband spectrum by Artificial Intelligence (AI) pipelines. However, direct sampling of other electronics-only solutions is unsuitable for simultaneous processing of low-RF to FR3 band (24 GHz). We propose combining CMOS electronic circuits with silicon-based photonic integrated circuits (PICs) to enable novel broadband RF photonic channelizers. This work presents a system-level design and analysis of a channelizer using on-PIC optical filter banks and optical-domain demodulation.

Index Terms—Analog optical link, Photonic Integrated Circuit (PIC), RF Photonics, RF-to-optical modulator, Silicon Photonics.

I. INTRODUCTION

THE demand for wideband operation in future wireless communications, the Internet of Things (IoT), imaging, sensing, and electronic warfare necessitates advanced spectrum management through integrated electronics. AI-driven distributed systems further require low-cost, power-efficient solutions for processing wideband signals.

Direct sampling of the entire spectrum of interest from DC to 24GHz and channelization in the digital domain is the architecturally simplest approach. However, this will require a Nyquist rate analog-to-digital converter (ADC) with over 48 GHz sampling rate. Such ADCs, realized using time-interleaved architectures, are prohibitively expensive and power-intensive with their effective number of bits (ENOB) limited by the sampling jitter to around 6-bits. In principle, an analog filter bank could be used to decompose a wideband signal into multiple narrower sub-bands, which could then be downconverted to the baseband using a bank of RF mixers. Alternatively, mixer-bank-based [1] or frequency-folded [2] architecture can be employed. However, these electronic architectures are limited to below 1GHz bandwidth.

Besides limited bandwidth, the key limitation of traditional analog approaches is that active IC-based signal processing introduces significant noise and linearity challenges. Our approach explores recent breakthroughs in photonic integrated circuit (PIC) technology to overcome the inherent bandwidth, noise, and linearity constraints of conventional on-chip analog electronic sub-banding techniques for wideband spectrum.

The advent of Silicon Photonic (SiP) integrated circuits and their fabrication on multi-project wafer (MPW) platforms is enabling the integration of complete optoelectronic systems within a single chip-scale package. RF photonics, a well-

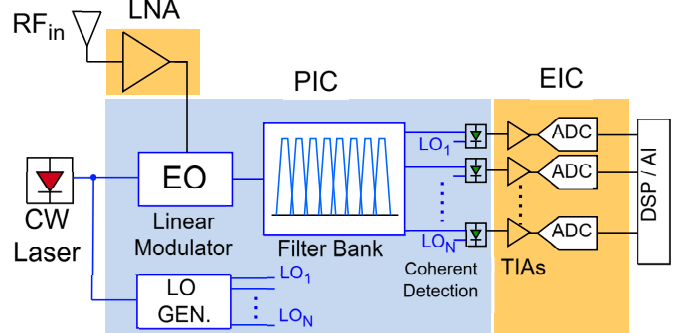


Fig. 1. RF Photonic channelizer architecture.

established field, processes RF signals using discrete lasers, modulators, and photodetectors before transmission over optical fiber. Beyond the inherent advantages in size, weight, power, and cost (**SWaPc**), novel PICs offer solutions to longstanding limitations of discrete optoelectronic systems.

This article presents the system-level design of an integrated RF photonic channelizer for broadband spectrum perception. The remainder of the manuscript is structured as follows: Section II details the overall architecture and circuit components. Section III provides noise analysis and simulation results outlining fundamental trade-offs in the on-PIC link budget, followed by the conclusion.

II. RF PHOTONIC CHANNELIZER ARCHITECTURE

This work investigates an RF photonic channelization from near DC to the edge of the FR3 band (24GHz), and down-conversion architecture as shown in *Fig. 1*. Most signal processing is performed in the optical domain on a PIC. In this coherent processing architecture, the continuous-wave (CW) laser at 1550nm is split into two paths: one for modulation and another for optical local oscillator (LO) generation. The input RF spectrum is amplified using a broadband low-noise amplifier (LNA). The RF modulation of the laser is performed using a lithium niobate electro-optic (EO) modulator for high linearity.

An optical filter bank then processes the modulated optical spectrum realized using arrayed waveguide grating (AWG) with $N=8$ channels of $B=3$ GHz spacing, ranging from DC to 24 GHz. The sub-banded channels from the PIC realization of a wideband filter bank can be sub-sampled using an ADC with $\geq B$ sampling rate for achieving wideband functionality through multiple sub-bands in the digital signal processor

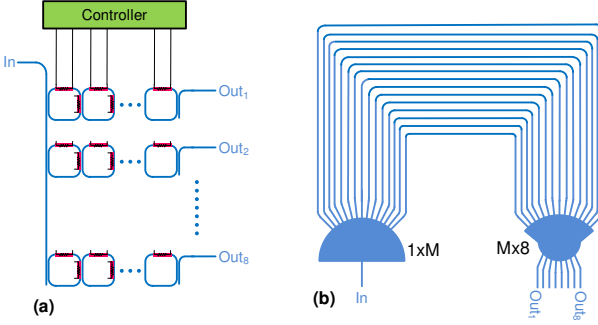


Fig. 2. (a) Channelizer based on CROW filters, (b) Arrayed Waveguide Grating (AWG). Replace this by your plot from Lumerical Interconnect.

(DSP). However, the curse of sub-sampling is that it suffers from noise aliasing effect, *i.e.*, where out-of-band noise is aliased into the band of interest). Moreover, this would require the transimpedance amplifiers (**TIA**) with sufficient bandwidth to process the entire $N \times B$ bandwidth, with a resulting reduction in optical sensitivity due to broadband thermal noise ($kTNB$).

Optical-domain downconversion is an alternative approach, where coherent detection is performed for each channel. However, this approach would require N optical LOs to be used with the 90° optical hybrid. Finally, the downconverted signals are in the form of photocurrents, which are then processed by linear TIAs. The advantage of this approach is that the linear TIAs need to process only B bandwidth with lower in-band noise (kTB) and significantly reduced power consumption.

A. RF to Optical Modulation

In the proposed system, the input RF signal is first routed through a wideband and linear LNA with a bandwidth of 24 GHz. Even though some RF photonic systems avoid the LNA in the interest of linearity, the LNA improves the link noise figure (**NF**) while compensating for the inherent photonic losses, ensuring that the signal maintains a sufficient signal-to-noise ratio (**SNR**) for subsequent processing stages. Following amplification, the signal is directed to a Mach-Zehnder Modulator, which converts the RF signal into the optical domain. However, Dual-Parallel Mach-Zender Modulator (**DP-MZM**) is proven to have better linearity over the standard MZM, as it cancels even order distortion and with low third-order intermodulation distortion (**IM3**) resulting in a desirable spur-free dynamic range (**SFDR**) >100 dB $^{2/3}$ across the entire range of spectrum of interest [3] [4]. Notably, the DP-MZM supports single-sideband (**SSB**) modulation.

B. Optical Filter Bank

The broadband RF-modulated optical signal is processed by a photonic filter bank as seen in **Fig. 1**. Optical filters can be designed on a PIC with high selectivity and >20 dB out-of-band suppression. Since passive optical circuits are inherently linear and broadband, they far surpass the filtering achieved in electronic realization. The photonic filter bank can be realized using a cascaded Mach-Zehnder interferometer (**MZI**) or ring-based filters. Ring-based filters can use coupled-resonator optical waveguides (**CROW**), shown in **Fig. 2(a)**, where resonators are

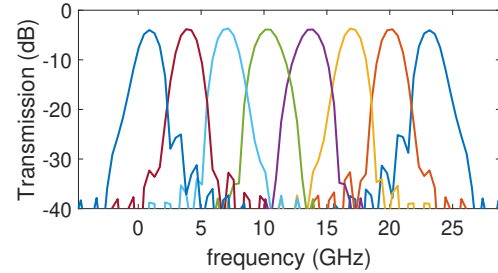


Fig. 3. Simulated AWG spectrum for $N=8$ channels with separation of 3GHz.

coupled through waveguides to synthesize sharp optical filter responses [5]. While CROWs are compact and on-PIC filters with automatic tuning have been demonstrated [6], an 8-channel filter bank will need ≥ 24 rings. Tuning coupling and resonances of each ring, especially with on-chip thermal crosstalk, will lead to a complex controller design. MZI-based channelizers are attractive but exhibit lower out-of-band rejection [7].

In our architecture, we propose to use arrayed waveguide grating (AWG) shown in **Fig. 2(b)**, which require a smaller number of tuning elements and exhibit lower loss. The AWG splits the input into M waveguides with progressively increasing group delay of ΔL . These waveguides are combined with a free-space $M \times N$ star coupler, resulting in the $N=8$ equally spaced outputs. The frequency spacing is given by

$$\Delta f_{min} = \frac{c}{n_g N \Delta L} \quad (1)$$

where n_g is the group index of the waveguides. **Table I** compares recent PIC-based AWGs for RF photonic applications. For GHz frequency spacing, the PIC area becomes very large with associated losses and cost [8]. Recent work used a low-loss silicon nitride (SiN) process, associated with a large bend radius ($>100\mu\text{m}$) leading to a large PIC area [9]. In our architecture, we are using Si waveguides in an ultra-low-loss SiP process with $< 1\text{dB/cm}$ loss. The simulated spectral response is shown in **Fig. 3**. This allows tighter bends ($10\mu\text{m}$) with compact serpentine routing of the waveguides leading to a manageable estimated PIC area of $4\text{mm} \times 3\text{mm}$.

TABLE I
COMPARISON OF SiP AWGS FOR RF PHOTONIC APPLICATIONS.

Ref.	Channel Spacing	Num of Channels	Num of WGs	Technology	Area
[8]	50 GHz	11	35	1 μm Si WG	4mm \times 4mm
	10 GHz				11mm \times 4mm
	1GHz				9mm \times 12mm
[9]	3.9 GHz	10	33	Low-loss SiN WG	12.5mm \times 19.5mm
This work	3 GHz	8	16	Low-loss 0.5 μm Si WG	4mm \times 3mm (Estimated)

C. Optical Coherent Downconversion

Coherent optical detection beats the optical signal, P_s , with the optical local oscillator (**LO**) signal, P_{LO} , resulting in an output current [10]

$$I_{out}(t) = 2\rho \sqrt{P_s(t) \cdot P_{LO}} \quad (2)$$

Coherent downconversion is performed using a 180° coupler and a pair of photodiodes as depicted in **Fig. 4 (a)** [11].

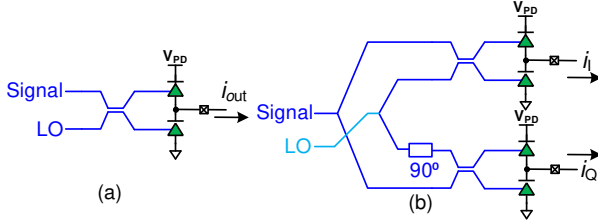


Fig. 4. Balanced Detection Implementations. (a) In-phase Balanced Detection. (b) I/Q Balanced Detection.

However, a small phase mismatch between LO and Signal leads to random scaling of the downconverted signal. Using the balanced detection scheme, seen in **Fig. 4 (b)**, results in in-phase and quadrature (I/Q) components, ρ being the detector responsivity:

$$I_I(t) = 2\rho \sqrt{P_S(t) \cdot P_{LO}} \cdot \cos(\theta_{sig}(t) - \theta_{LO}) \quad (3)$$

$$I_Q(t) = 2\rho \sqrt{P_S(t) \cdot P_{LO}} \cdot \sin(\theta_{sig}(t) - \theta_{LO}) \quad (4)$$

Digital Signal Processing (DSP) techniques are used to recover both magnitude and phase data from the I/Q signals [12]. Alternatively, analog domain squaring and summing can be used to recover the envelope as $I_{env} = \sqrt{I_I^2 + I_Q^2} = 2\rho \sqrt{P_S(t) \cdot P_{LO}}$ [13]. I/Q Balanced Detection is used in the proposed system.

D. Linear TIAs

A linear transimpedance amplifier (TIA) with high linearity and low noise is crucial for accurately converting photodetector currents to the voltage domain. **Fig. 5** shows a linear TIA circuit realized in 65nm CMOS technology. A resistive feedback CMOS inverter topology is used for linearity followed by linear programmable gain stages and output buffers to interface with off-chip ADCs [14]. A DC offset cancellation (DCOC) loop is needed to set the output common-mode voltage and cancel any mismatches of the PDs. Preliminary simulations shown in **Fig. 6** predict a TIA gain of $R_T=63 \text{ dB}\Omega$ for a $B=3\text{GHz}$ bandwidth with an input referred noise of $i_{n,TIA} = 3.1\text{pA}/\sqrt{\text{Hz}}$.

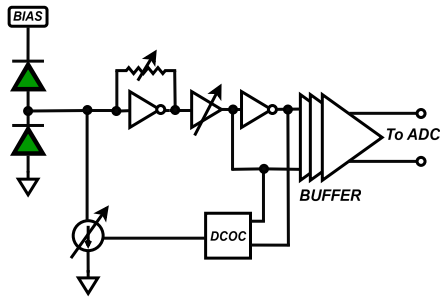


Fig. 5. A linear TIA circuit to process the downconverted optical signals.

III. SYSTEM-LEVEL NOISE ANALYSIS

In this section, we estimate the noise contributions from the individual blocks in the channelizer and analyze their impact on the overall performance.

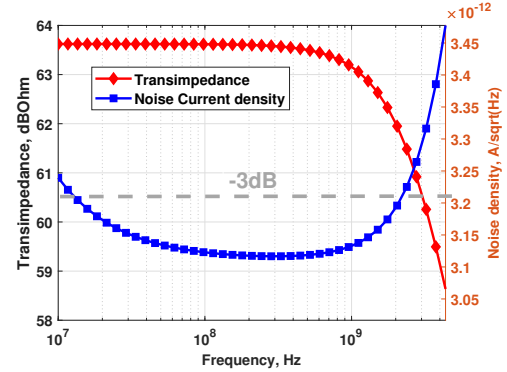


Fig. 6. Simulated TIA gain and noise response.

A. Noise sources

1) MZM noise

The MZM is impedance-matched with the RF source. Neglecting the electrode loss, the MZM noise contribution in each channel is estimated as kTB [15].

2) Photodetector noise

Photodetectors (PDs) generate shot noise and thermal noise in the RF photonic front end. Shot noise is dependent on the DC component in the output current, I_D , and is given by $P_{shot} = i_{sn}^2 B = 2qI_D B$. The thermal noise contribution is negligible [15], [16].

3) Laser Relative Intensity Noise

The laser's Relative Intensity Noise (RIN) is due to the random emission of the stimulated photons. The effect of RIN is observed in the photodetector output and depends on I_D^2 . The RIN noise contribution is given as [15], [16]

$$P_{RIN} = i_{rin}^2 B = 10^{\left(\frac{RIN}{10}\right)} I_D^2 B \quad (5)$$

4) TIA noise

The input referred noise from the TIA, $P_{n,TIA} = i_{n,TIA}^2 B$, includes the thermal and flicker noise contributions [17].

B. Balanced Detection Noise Analysis

Fig. 7 depicts the noise model for the entire channelizer. The noise in a balanced detector is estimated differently from an intensity-modulated link. The shot noise and RIN noise depend on the DC component of the subtracted output currents. If the same laser source is used as desired, the RIN noise in both the PDs are closely correlated. Therefore the RIN noise currents will be subtracted. Since the shot noise in the two PDs is uncorrelated, the currents will be added [18].

Since the DC current in both the PDs is due to the LO and signal power ($P_s = \frac{T_f P_L}{L_c}$), the shot and RIN noise powers can be written as [19]

$$\begin{aligned} P_{RIN} &= 10^{\left(\frac{RIN}{10}\right)} P_{LO}^2 (\rho_1 \kappa - \rho_2 (1 - \kappa))^2 B \\ &= 10^{\left(\frac{RIN}{10}\right)} P_{LO}^2 [\rho \Delta \kappa + \Delta \rho (1 - \Delta \kappa)]^2 \cdot B \rightarrow 0 \end{aligned} \quad (6)$$

$$\begin{aligned} P_{shot} &= 2qP_{LO}(\rho_1 \kappa + \rho_2 (1 - \kappa))B + \frac{\kappa P_s B}{2} \kappa P_s / 2 \\ &\approx 2qP_{LO}\rho B + \frac{\kappa P_s B}{2} \end{aligned} \quad (7)$$

REFERENCES

- [1] V. K. Singh, W.-G. Ho, and R. Gharpurey, "A frequency-folded adc channelizer with digital equalization and relaxed anti-alias filtering," *IEEE Transactions on Circuits and Systems I: Regular Papers*, vol. 65, no. 7, pp. 2304–2317, 2018.
- [2] V. Singh, T. Forbes, W.-G. Ho, J. Ko, and R. Gharpurey, "A 16-band channelizer employing harmonic rejection mixers with enhanced image rejection," in *Proceedings of the IEEE 2014 Custom Integrated Circuits Conference*. IEEE, 2014, pp. 1–4.
- [3] X. Huang, Y. Liu, D. Tu, Z. Yu, Q. Wei, and Z. Li, "Linearity-enhanced dual-parallel mach-zehnder modulators based on a thin-film lithium niobate platform," in *Photonics*, vol. 9, no. 3. MDPI, 2022, p. 197.
- [4] Y. Gu and J. Yao, "Microwave photonic link with improved dynamic range through π phase shift of the optical carrier band," *Journal of Lightwave Technology*, vol. 37, no. 3, pp. 964–970, 2019.
- [5] Z. Wan, X. Xie, Q. Cen, Y. Ding, J. Xia, K. Xu, M. Li, and Y. Dai, "Photonics-assisted rf channelizer based on integrated ring modulator," *Journal of Lightwave Technology*, 2024.
- [6] M. J. Shawon and V. Saxena, "Fully automatic in-situ reconfiguration of optical filters in a cmos-compatible silicon photonic process," *Journal of Lightwave Technology*, vol. 41, no. 5, pp. 1286–1297, 2022.
- [7] C.-H. Chen and Y.-J. Hung, "5 ghz optical channelizer based on cascaded mach-zehnder interferometers on soi," in *2022 27th OptoElectronics and Communications Conference (OECC) and 2022 International Conference on Photonics in Switching and Computing (PSC)*. IEEE, 2022, pp. 1–3.
- [8] M. Gehl, D. Trotter, A. Starbuck, A. Pomerene, A. Lentine, and C. DeRose, "Active phase correction of high resolution silicon photonic arrayed waveguide gratings," *Optics Express*, vol. 25, no. 6, pp. 6320–6334, 2017.
- [9] F. Gambini, R. Moreira, D. Robles, A. Gambacorta, and M. Stephen, "An ultra-compact, narrow-bandwidth, and high-density channel photonic integrated channelizer based on serial arrayed waveguide grating architecture," *Journal of Lightwave Technology*, vol. 42, no. 8, pp. 2908–2916, 2024.
- [10] K. Kikuchi, "Fundamentals of coherent optical fiber communications," *Journal of lightwave technology*, vol. 34, no. 1, pp. 157–179, 2015.
- [11] ———, "Coherent optical communications: Historical perspectives and future directions," *High Spectral Density Optical Communication Technologies*, pp. 11–49, 2010.
- [12] M. Kuschnerov, F. N. Hauske, K. Piyawanno, B. Spinnler, M. S. Alfiad, A. Napoli, and B. Lankl, "Dsp for coherent single-carrier receivers," *Journal of lightwave technology*, vol. 27, no. 16, pp. 3614–3622, 2009.
- [13] B. Schrenk, "Photonic signal processing for phase-agnostic coherent optical reception," *Journal of Lightwave Technology*, 2024.
- [14] V. Saxena, A. Kumar, S. Mishra, S. Palermo, and K. R. Lakshmikumar, "Optical interconnects using hybrid integration of cmos and silicon-photonic ics," *IEEE Transactions on Circuits and Systems II: Express Briefs*, vol. 71, no. 3, pp. 1632–1637, 2023.
- [15] C. H. Cox, *Analog optical links: theory and practice*. Cambridge University Press, 2006.
- [16] D. Marpaung, "High dynamic range analog photonic links design and implementation," *University of Twente*, 2009.
- [17] E. Sackinger, *Broadband Circuits for Optical Fiber Communication*, 1st ed. Wiley, 2005.
- [18] C. Wang and L. Gao, "Investigation of balanced detection and receiver for coherent lidar," in *International Symposium on Photoelectronic Detection and Imaging 2009: Laser Sensing and Imaging*, vol. 7382. SPIE, 2009, pp. 164–171.
- [19] P. Zhang, Z. Tan, Z. Ding, and L. Guo, "Simulation analysis of balance detection technique in coherent optical receiver," *Optics and Photonics Journal*, vol. 11, no. 8, pp. 301–313, 2021.
- [20] Y. Painchaud, M. Poulin, M. Morin, and M. Tétu, "Performance of balanced detection in a coherent receiver," *Optics express*, vol. 17, no. 5, pp. 3659–3672, 2009.
- [21] M. J. Shawon and V. Saxena, "Analysis of trade-offs in rf photonic links based on multi-bias tuning of silicon photonic ring-assisted mach zehnder modulators," *arXiv preprint arXiv:2110.02737*, 2021.